**PAPER**

Check for updates

## Microneedle-assisted transdermal delivery of carvedilol nanosuspension for the treatment of hypertension

Anushri Deshpande,* Vidhi Mer, Darshana Patel and Hetal Thakkar [iD]

Carvedilol nanosuspension loaded microneedles patch was formulated and characterized by particle size, zeta potential, solubility, Transmission Electron Microscopy, X-Ray Diffraction, in-vitro release and *in-vivo* pharmacokinetic studies A nanosuspension-loaded microneedle patch was successfully prepared and characterized by optical microscopy, scanning electron microscopy, axial fracture force, *in vitro* dissolution study, % drug content, *in vitro* drug-release study, *ex vivo* studies, an *in vivo* study, and stability studies. The particle size, PDI, and zeta potential of the carvedilol nanosuspension were found to be 179.6 $\pm$ 1.15 nm, 0.163 $\pm$ 0.01, and $-14.2 \pm 0.55$ mV, respectively. There was a 9.21-fold increase in the saturation solubility of the carvedilol nanosuspension. Nanosuspension-loaded microneedles contained 98.78 $\pm$ 0.12% carvedilol. The relative bioavailability of the carvedilol from the microneedle patch was found to be 2.82-fold higher compared to the marketed formulation. The drug release from the microneedles followed zero-order kinetics, which is desirable in the case of transdermal delivery. The stability study indicated that the prepared formulation was stable under the storage conditions used. Thus, the developed transdermal microneedle patch containing the carvedilol nanosuspension seems to be a promising approach to foster greater patient compliance for the management of hypertension.

## 1. Introduction

Oral delivery is considered to be the most patient-compliant route for drug administration. However, certain limitations such as high first-pass metabolism, low oral bioavailability, and GI disturbance necessitate the exploration of alternative routes for drug delivery. The transdermal drug delivery system is associated with several advantages such as elimination of first-pass metabolism, the possibility of controlled release, and facile administration of a therapy.

Carvedilol is a biopharmaceutics classification system (BCS) class II drug used in the management of hypertension, cardiac arrhythmias, angina pectoris, and symptomatic heart failure.[1] Carvedilol is available in tablet form with strengths of 3.125 mg, 6.25 mg, 12.5 mg, and 25 mg. The plasma half-life of carvedilol is 6–10 h, which may necessitate a higher frequency of administration.[2] Due to this limitation, controlled- and sustained-release formulations have been developed. Some of them are controlled-release tablets[3] and pellets[4] composed of hydroxypropyl methylcellulose, eudragit, or ethyl cellulose. Due to its low solubility and high first-pass metabolism,

*The Maharaja Sayajirao University Of Baroda, Vadodara, India.*
*E-mail: hetal.thakkar-pharmacy@msubaroda.ac.in*

the oral bioavailability of carvedilol is low, at 25–30%. The oral bioavailability of a poorly water-soluble drug undergoing high first-pass metabolism can be enhanced by various approaches. Some of the approaches reported for carvedilol are solid lipid nanoparticles,[5] niosomal carriers,[6] solid self-nanoemulsifying drug delivery systems (S-SNEDDS),[7] nanosuspension from an osmotic pump capsule,[8] and solid dispersions.[9]

A nanosuspension is one of the approaches used for the enhancement of drug solubility.[10] It has many advantages such as a simple method of preparation, less requirement of excipients, increased dissolution velocity and saturation solubility, improved adhesion, increased bioavailability leading to a decrease in the dose and fast-fed variability, and ease of large-scale manufacturing. The availability of the drug in nanosize leads to enhanced solubility due to a large increase in the surface area.[11] Thus, it was expected that a nanosuspension of carvedilol would have greater solubility and consequently higher systemic absorption.

Transdermal drug delivery can overcome the limitations of oral and parenteral administration. However, this route is currently useful for only a small number of drugs, due to the impermeability of the outer layer of skin, the stratum corneum (SC).[12] A penetration enhancement approach is usually required when pursuing transdermal drug delivery to achieve a desirable plasma concentration.[13] Various penetration

enhancement techniques have been reported, such as ionto-phoresis,[14] sonoporation,[15] microneedles,[16] and chemical enhancers.[17]

MNs are minimally invasive devices that bypass the SC barrier of the skin, and thus, the dermal microcirculation and inferior layers of the skin can be accessed. When applied to the skin, they painlessly puncture the SC, creating microscopic channels through which drugs can diffuse. This provides a physical pathway for drugs to permeate the skin in a much higher concentration as compared to a normal topical formulation. Soluble MNs are composed of polymers that are biodegradable, biocompatible, and solubilize upon insertion into the skin. Thus, they reduce the risk of toxic or biohazardous waste.

Polymers such as poly(methyl vinyl ether-*co*-maleic acid),[18,19] chitosan,[20] and polyvinyl alcohol[21] form a hydrogel when they come in contact with the interstitial fluid of the SC, and they are used for the preparation of microneedles. Once in the skin, they swell, thus creating a porous network through which drugs contained within a reservoir can diffuse, and subsequently move into the dermal microcirculation. Thus, they control the rate of drug release.

Amongst the different polymers available for microneedle preparation, poly(methyl vinyl ether-*co*-maleic anhydride) was selected due to its desirable properties such as biodegradable nature, capacity to form a hydrogel, bioadhesiveness, and ability to provide sustained release of a drug. The development of soluble microneedles for lipophilic drugs is challenging due to the uneven distribution of a drug in the microneedle matrix because of its insoluble nature. The non-uniform size of drug particles leads to the formation of imperfect microneedles. Formulation of a nanosuspension leads to uniformly sized particles and increased aqueous solubility, which allows for more rapid absorption into the systemic circulation. Thus, the principal objective of the present research was to formulate and evaluate carvedilol-loaded microneedles by *in vitro*, *ex vivo*, and *in vivo* studies and determine their ability to increase the bioavailability.

# 2. Materials and methods

## 2.1 Materials

Carvedilol was received as a gift from Zydus Pharmaceuticals Limited, Ahmedabad, India. Sodium deoxycholate (NaDC) and polymethyl vinyl ether-*alt*-maleic anhydride (PMVE/MA) were purchased from Sigma-Aldrich, India. Zirmil® (zirconium oxide) beads 0.4 mm in diameter were purchased from Magnum Apex, India, and Sylgard® 184: polydimethylsiloxane (PDMS) was procured from Dow Corning, USA. Potassium dihydrogen phosphate and sodium lauryl sulphate (SLS) were purchased from Fisher Scientific, India and sodium chloride was purchased from Sulab Chemicals, India. Disodium hydrogen phosphate and sodium hydroxide were purchased from Astron, India.

## 2.2 Methods

### 2.2.1 Formulation of the carvedilol nanosuspension.
A wet media milling technique was used to prepare the nanosuspension using Zirmil® (zirconium oxide) beads.[22] In this technique, zirconium oxide beads were used as milling agents to formulate the nanosuspension. The composition of the nanosuspension and screening of the surfactants are given in Tables 5 and 6, respectively. First, 0.5% NaDC was dissolved in 5 mL of distilled water in a 10 mL glass vial, and 50 mg of carvedilol was added to this solution. Then, 10 g of zirconium beads was added, and the solution was stirred on a magnetic stirrer at 1000 rpm for 4 hours. The prepared batch was then separated from the zirconium oxide beads using a 100-mesh sieve. This method was optimized using a $3^2$ full factorial design (data not shown).

### 2.2.2 Preparation of microneedle molds.
To prepare the microneedle mold derma stamp, 36 titanium needles 1.5 mm in length were used as a master structure. Polydimethylsiloxane (PDMS) and curing agent in a 10:1 weight ratio were added to the molding container and carefully mixed to prevent the formation of air bubbles. The air bubbles were removed by placing the mold in a vacuum desiccator for five minutes. After removal of the air bubbles, the MN derma stamp was vertically inserted and maintained overnight in this PDMS solution. The derma stamp was later removed from the molding container, and the container was maintained at 90 °C in a water bath for 5 hours. After completely curing, the mold was removed from the molding container.

### 2.2.3 Formulation of carvedilol nanosuspension-loaded microneedles.
The composition of the nanosuspension-loaded microneedles is given in Table 5. PMVE/MA polymer was used to prepare a sustained-release MN patch.[24] Different concentrations of polymer blends were prepared by adding PMVE/MA to the previously prepared carvedilol nanosuspension. To this solution, 100 μL of glycerin was added as a plasticizer. The PDMS MN molds were filled with these dispersions.[23] Then, the molds were centrifuged at 3000 rpm for 3 cycles at 15 minutes each. This ensured the forceful filling of the dispersion in the tiny microneedle cavities of the molds. Later, the molds were maintained in a vacuum desiccator for 24 hours to ensure the complete drying of the MN patch. After 24 hours, the MN patches were removed from the molds using two-sided adhesive tape and preserved under a vacuum desiccator until further characterization.[24]

**Table 1** Microneedle dimensions as per scanning electron microscopy (SEM)

| Characterization | Observed value | Reference value |
|---|---|---|
| Length | 1.5–2 mm | 0.15–2.5 mm |
| Tip diameter | 5 μm | 1–25 μm |
| Base diameter | 260–400 μm | 50–250 μm |
| Distance between two needles | 581 μm | 500–800 μm |

**Table 2** Correlation coefficient ($R^2$) values of kinetic models

| Formulation | Regression coefficient ($R^2$) | | | | |
| --- | --- | --- | --- | --- | --- |
| | Zero order | First order | Higuchi model | Hixson–Crowell model | Korsemeyer–Peppas model |
| Microneedles | 0.9928 | 0.9468 | 0.916 | 0.9823 | 0.9823 |

**Table 3** Pharmacokinetic parameters of different formulations

| Pharmacokinetic parameters | Marketed oral tablet | Simple transdermal patch | Microneedle patch |
| --- | --- | --- | --- |
| $C_{max}$ (ng ml$^{-1}$) | 432.3 ± 20 | 589.3 ± 16 | 727.4 ± 18 |
| $T_{max}$ (h) | 6 | 6 | 6 |
| AUC (ng ml$^{-1}$ h$^{-1}$) | 4299 | 5686 | 12 136 |
| $t_{1/2}$ (h) | 6.19 | 5.84 | 9.7 |
| MRT (h) | 11.10 | 11.47 | 17.24 |
| Relative bioavailability | — | 1.32 | 2.82 |

**Table 4** AFF, % drug content, and % CDR to assess the stability of samples at room temperature and at refrigeration temperature

| | AFF (N) | Drug content (%) | % CDR in 24 hours |
| --- | --- | --- | --- |
| (25–40 °C) | | | |
| Initial | 5.3 ± 0.06 | 97.92 ± 0.52 | 91.55% |
| After 15 days | 5.1 ± 0.03 | 96.24 ± 0.22 | 89.65% |
| After 30 days | 4.81 ± 0.09 | 95.89 ± 0.61 | 86.25% |
| (2–8 °C) | | | |
| After 15 days | 5.34 ± 0.06 | 97.56 ± 0.32 | 91.25% |
| After 30 days | 5.08 ± 0.04 | 96.58 ± 0.12 | 89.15% |
| After 30 days | 4.88 ± 0.05 | 94.65 ± 0.57 | 86.57% |

**Table 5** Composition of the nanosuspension and nanosuspension-loaded microneedles

| Ingredients | Concentration |
| --- | --- |
| Composition of nanosuspension | |
| Sodium deoxycholate (NaDC) | 0.5% |
| Distilled water | 5 mL |
| Carvedilol | 50 mg |
| Composition of nanosuspension-loaded microneedles | |
| Volume of nanosuspension in a single patch | 300 µL |
| Poly(methyl vinyl ether-*alt*-maleic anhydride) (PMVE/MA) | 20% |
| Glycerin | 100 µL |

### 2.3 Characterization of the carvedilol nanosuspension

**2.3.1 Particle size and zeta potential analysis.** Particle size and zeta potential were measured using a Malvern Zeta Sizer (Nano-ZS). For analysis, the formulation was appropriately diluted with distilled water and added to clear disposable sample cuvettes for recording the particle size and PDI. The zeta potential of the nanosuspension was also recorded using a Malvern Zeta Sizer (Nano-ZS)[25]

**2.3.2 Saturated solubility.** The carvedilol nanosuspension was added to 10 mL of phosphate-buffered saline (PBS, pH 7.4) until saturation and stirred at room temperature for 24 hours. It was then centrifuged at 5000 rpm for 15 minutes, and the obtained supernatant was removed by aspiration and purified using a 0.22-µm filter. The sample was suitably diluted with PBS (pH 7.4) before measuring its absorbance using a UV spectrophotometer (UV 1800, Shimadzu, Japan) at a wavelength of 242 nm. The saturated solubility in PBS (pH 7.4) containing 2% SLS was then calculated from the calibration plot.[25]

**2.3.3 Transmission electron microscopy (TEM).** A drop of diluted carvedilol nanosuspension was placed on a carbon film coated on a copper grid and allowed to air dry. The grid was placed in the sample probe inserted into the transmission electron microscope (Technai, Philips Holland, SICART), and the results were recorded.[25]

**2.3.4 X-ray diffraction (XRD).** An X-ray diffractometer (Bruker, Germany) was used to obtain X-ray diffraction patterns of pure carvedilol and its lyophilized nanosuspension. The samples were measured in the $2\theta$ angle range between 5° and 90° with a scanning rate of 3° per minute and a step size of 0.02°.[26]

**2.3.5 Energy dispersive X-ray spectroscopy (EDS).** EDS (JSM- 5610 V, JEOL, Japan) is used to separate the characteristic X-rays of different elements into an energy spectrum. EDS software was used for analysis to determine the abundance of specific elements. EDS was used to quantify the zirconium in the nanosuspension. An EDS system is typically integrated into

**Table 6** Screening of surfactants

| Sr. no. | Surfactant | Concentration of surfactant (%w/v) | Amount of drug (mg) | Size (nm) | PDI | Solubility (µg ml$^{-1}$) |
| --- | --- | --- | --- | --- | --- | --- |
| 1 | Poloxomer 407 | 0.5 | 50 | 450.9 | 0.235 | 30.56 |
| 2 | Poloxomer 188 | 0.5 | 50 | 401.9 | 0.2 | 25.8 |
| 3 | Polyvinyl alcohol (PVA) | 0.5 | 50 | 303.3 | 0.141 | 33.8 |
| 4 | Sodium taurocholate | 0.5 | 50 | 512.3 | 0.232 | 25.9 |
| 5 | Sodium cholate | 0.5 | 50 | 463.9 | 0.383 | 21.98 |
| 6 | Sodium deoxycholate (NaDC) | 0.5 | 50 | 189.5 | 0.129 | 51.47 |

SEM. A drop of nanosuspension was placed on the stubs, and it was dried in a dryer before it was analyzed.

## 2.4   Characterization of nanosuspension-loaded microneedles

**2.4.1   Optical microscopy.** A Nikon Eclipse inverted microscope with image processing and analysis software was used for the physical characterization of the polymeric microneedles.[27]

**2.4.2   Scanning electron microscopy (SEM).** For accurate measurement of the microneedle length and base diameter, SEM (JSM-5610V, JEOL, Japan) was used. The samples were horizontally attached to sample stubs to view the needle length, and software was used to measure the diameter of the base and needle length.[24]

**2.4.3   Axial fracture force (AFF).** A CT3 texture analyzer (Brookfield, USA) instrument was used to measure the axial fracture force. The MN patch was adhered to a fixed cylindrical platform, and another cylindrical probe (TA-39: 2 mm diameter) was used to compress the single MN patch on each occasion. A graph of force (g) *versus* distance (mm) was obtained by utilizing TexturePro CT software. A sudden decrease in force was considered a needle-breaking point, and the force at this point was recorded as a needle-fracture force.[28]

**2.4.4   *In vitro* dissolution study.** For conducting an *in vitro* dissolution study of MNs, a gelatin film with a hydration level of 35% was prepared. To prepare the gelatin film, 6.5 g of gelatin was hydrated in 10 mL of water for approximately 30 minutes. Then, the gelatin was dissolved at 60 °C in a water bath with continuous stirring. The solution was transferred to a glass Petri dish, and water was allowed to evaporate up to 10 g of the final weight. After evaporation, the gelatin film was cut into small square pieces. An optimized batch of microneedle patches was inserted into the gelatin film, removed after different time intervals (5 min, 10 min, 15 min, and 20 min), and then, the patches were viewed under a microscope.[29]

**2.4.5   Drug content (%).** The MN patch containing a nanosuspension equivalent to 5 mg of carvedilol was fully dissolved in 10 mL of PBS (pH 7.4) containing 2% SLS by slow stirring for 1–2 hours. Then, 1 mL of the above solution was withdrawn and diluted to 10 mL with PBS (pH 7.4) containing 2% SLS. Absorbance of the solution was recorded at 242 nm, and PBS (pH 7.4) containing 2% SLS was used as a blank.[27]

**2.4.6   *In vitro* drug release study.** An optimized batch of microneedles was inserted into an activated dialysis membrane and mounted between the receptor and donor chamber of a custom-made diffusion cell. It was mounted such that the tips of the microneedle patch pierced the dialysis membrane and were in contact with the release media, which consisted of PBS (pH 7.4) containing 2% SLS. The assembly was fixed on a magnetic stirrer and gently stirred throughout the test. A 1 mL sample was withdrawn at predetermined time intervals and was replaced with an equal volume of fresh PBS (pH 7.4). The drug concentration in the samples was estimated by UV spectrophotometer at a $\lambda_{max}$ of 242 nm. The release kinetics was studied using various models to analyze the obtained

data, and the model with the most optimal fitting was identified based on its regression coefficient ($R^2$) values.[24]

### 2.4.7   *Ex vivo* studies

*2.4.7.1   Drug permeation study.* Freshly excised rat abdominal skin was hydrated in PBS (pH 7.4) for 30 min before the study. Subcutaneous fat was removed with a scalpel, and the skin was placed on a stack of filter papers pre-wetted with PBS (pH 7.4) to provide mechanical support. Simple patches (composition: water, glycerin as a plasticizer, carvedilol, and PVME/MA polymer), as well as microneedle patches containing 5 mg of carvedilol, were applied onto the skin using gentle thumb pressure. The skin was immediately mounted between the donor and receptor chambers of the diffusion cell with the patch on the SC facing towards the donor side. The receptor chamber of the cell was filled with 7 mL PBS (pH 7.4) containing 2% SLS as a diffusion medium, and then, the liquid in the receptor chamber was subjected to gentle stirring using a magnetic stirrer. Next, 1 mL samples were withdrawn from the receptor compartment at predetermined time points over 24 hours, and were replenished with 1 mL of fresh diffusion medium. Quantitative estimation of the drug in the samples was performed using UV-visible spectrophotometry at 242 nm. The percentage of drug that permeated through the skin was calculated. A graph of the cumulative amount of drug that permeated as a function of time was generated, and the steady flux ($J_{ss}$, µg cm$^{-2}$ h$^{-1}$) was calculated from the slope of the linear portion of this graph. The permeation enhancement ratio (PER) compared to a plain patch (control) of PBS (pH 7.4) was calculated from the steady-state flux using the formula.[27]

*2.4.7.2   Drug retained on the surface of the skin.* At the end of 24 hours, the drug retained on the skin surface was estimated by washing the skin three times with PBS (pH 7.4) containing 2% SLS. These washings were collected, and the amount of drug present in them was estimated by UV-visible spectrophotometry at 242 nm. The drug deposited on the skin was calculated.[24]

*2.4.7.3   Drug retained within the skin.* After 24 hours, the washed skin was cut into small pieces using a chopper to estimate the drug deposition within the skin. The pieces were collected in diffusion media to extract the drug present in these pieces. The samples were then subject to homogenization (Remi homogenizer) for five minutes. This homogenized mixture was then subjected to a sonication in a bath sonicator for five 3 min cycles to extract the drug. The tissues were separated by centrifugation at 5000 rpm for 10 minutes. The supernatant was collected, and the drug present in it was analyzed by UV spectrophotometer at 242 nm after suitable dilution.[24]

*2.4.7.4   Transdermal flux.* The slope of the linear portion of the graph of the cumulative amount permeated as a function of time represents the steady-state flux ($J_{ss}$, µg cm$^{-2}$ h$^{-1}$). The permeation enhancement ratio (PER) was calculated from the steady-state flux using the following equation.

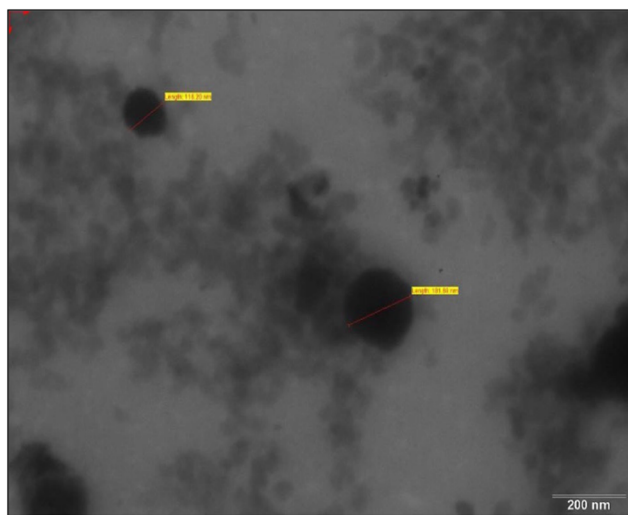$$PER = \frac{J_{ss}(\text{test})}{J_{ss}(\text{control})},$$

**Fig. 1** TEM of the carvedilol nanosuspension.

where, $J_{ss}$ (test) = steady-state flux obtained *via* an optimized microneedles patch, and $J_{ss}$ (control) = steady-state flux obtained *via* a simple transdermal patch.[24]

*2.4.7.5 Histopathology study.* The safety of breaching the SC with MNs was evaluated by performing a histopathology study. Rat abdominal skin was obtained by following protocol no: MSU/IAEC/2018-19/1806. Microneedles containing the drug or drug suspension were applied to freshly excised rat abdominal skin. A negative control and positive control were also prepared by treating rat skin with PBS (pH 7.4) and isopropyl alcohol (IPA), respectively, using the same method. After four hours, the skins were immersed in 10% buffered formalin (fixative), gradually dehydrated with increasing concentrations of ethanol, immersed in xylene, and finally embedded in paraffin. Then, 5-μm-thick sections of skin were cut from these paraffin blocks using a microtome, and the slices were placed on glass slides. The paraffin wax was removed by gently warming the slides and washing the molten wax with xylene. Sections were then washed with absolute alcohol and water and stained with hematoxylin and eosin to determine the histopathology. Commercial glycerol mounting fluid was used to finally
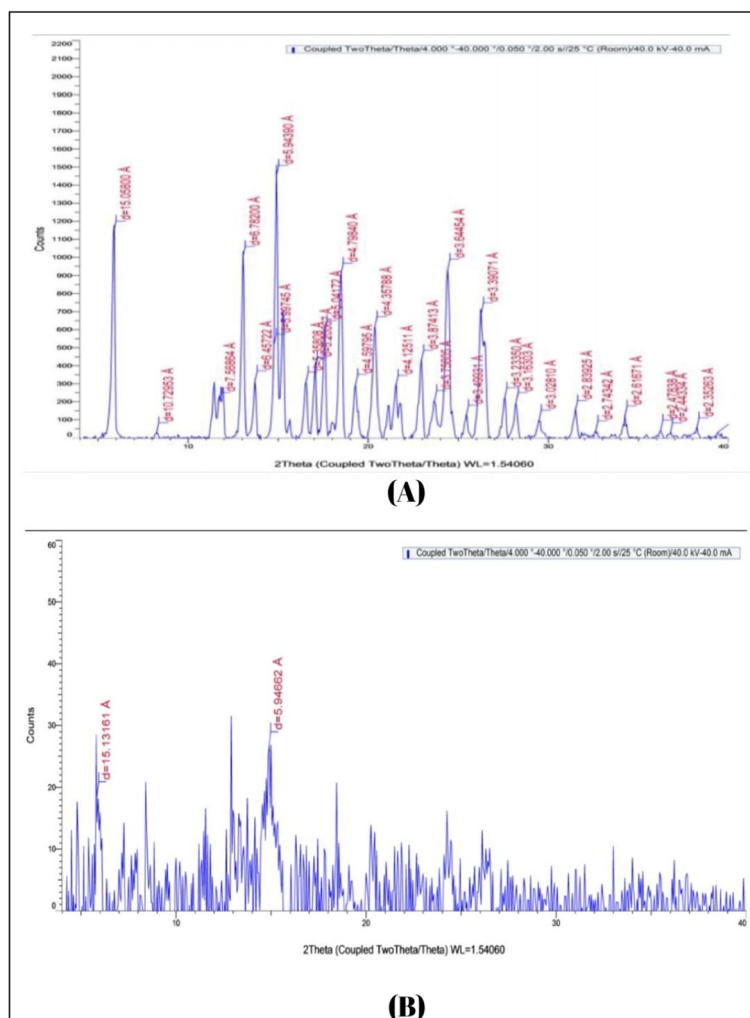


**Fig. 2** XRD of (A) pure carvedilol drug and (B) carvedilol nanosuspension.

mount the stained sections. The slides were analyzed at 10-fold magnification using an optical microscope.[30]

*2.4.7.6 In vivo studies.* The *in vivo* pharmacokinetic study was performed on male Wistar albino rats weighing 350–560 g. All animals were handled and housed according to CPCSEA guidelines, Department of Animal Welfare, government of India. The experimental protocol was approved by the Institutional Animal Ethics Committee (MSU/IAEC/2018-19/1824). Six sets of rats (3 animals in each set) were divided into 3 groups, with two sets of rats in each group. The oral suspension of carvedilol (0.5 mg kg$^{-1}$) was administered to Group 1. Groups 2 and 3 received a carvedilol simple patch (0.5 mg kg$^{-1}$) or a carvedilol MN patch, respectively. The marketed formulation of the carvedilol tablet was crushed and administered to rats fasted overnight as per the animal dose calculated (Group 1). The transdermal patch without microneedles and the microneedle patch were prepared according to animal dose and administered to Group 2 and Group 3, respectively.

The animal dose was calculated based on the following formula:

$$\text{Human equivalent dose} = \frac{\text{Animal dose}(\text{mg kg}^{-1})*\text{Animal factor (km)}}{\text{Human factor(km)}},$$

where the $K_m$ for rats was 6, and for humans (60 kg) was 37. Rat abdominal skin was shaved using a razor. Then, the 0.25 mg drug-loaded microneedle patch and a transdermal patch without microneedles were applied to the rat abdominal skin.

The volume of blood which can be withdrawn from a rat is limited and hence each group consisting of 6 animals were divided into 2 sets of 3 animals each. At the time intervals of 1 hour, 6 hours and 12 hours, set-1 animals were used while at the time intervals of 3 hours and 24 hours, set 2 animals were used. After blood collection, saline was administered to the rats for replenishment. These blood samples were centrifuged at 5000 rpm for 15 minutes at 4 °C. Then, plasma was separated as the supernatant and stored at 4 °C for further analysis by HPLC (Agilent, USA).[31] At the time of the protein analysis, samples were precipitated and analyzed by the developed HPLC method. A time *versus* plasma concentration graph was plotted to determine the pharmacokinetic parameters such as peak concentration ($C_{max}$), time to attain peak concentration ($T_{max}$), the area under the curve (AUC), and relative bioavailability.[24]

**2.3.1 Stability study.** The stability of carvedilol nanosuspension-loaded microneedle patches was examined under different storage conditions over 1 month.

(1) At refrigeration temperature (2–8 °C).

(2) At room temperature (25–40 °C): the optimized MN patches were placed in an airtight plastic container with a bag containing silica as a desiccant. The containers were then tightly closed and sealed using Parafilm M® and finally with aluminum foil to avoid contact with moisture. One container was stored at room temperature (25–40 °C), and the other one was refrigerated (2–8 °C). The stability study was conducted by comparing the characterization parameters of the MN patches: AFF, % drug content, and % cumulative drug release of the MN patches under both conditions after 15 days and 30 days.[24]

Spectrum processing:
No peaks omitted

Processing option: All elements analyzed (Normalised)
Number of iterations = 4

Standard:
C   CaCO3   1-Jun-1999 12:00 AM
O   SiO2    1-Jun-1999 12:00 AM

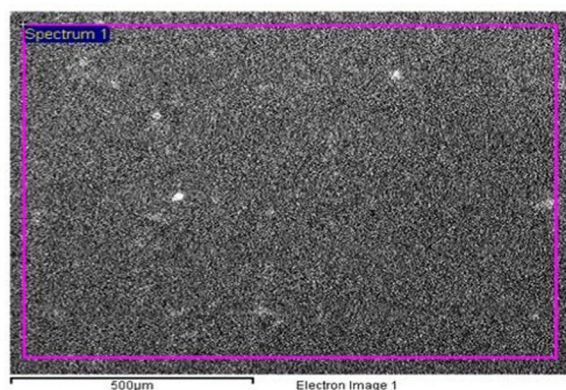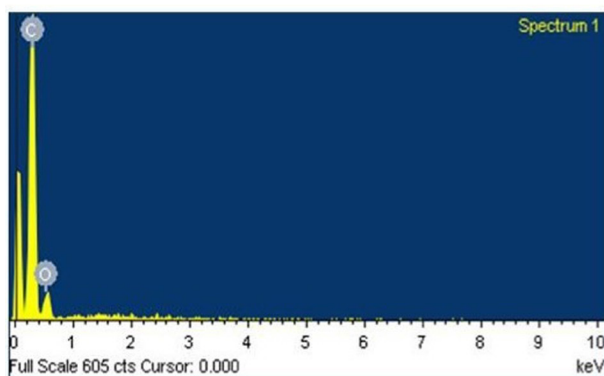| Element | Weight% | Atomic% |
|---------|---------|---------|
| C K | 76.86 | 81.56 |
| O K | 23.14 | 18.44 |
| Totals | 100.00 | |

**Fig. 3** EDS report for the nanosuspension.

# 3. Results and discussion

## 3.1 Nanosuspension analysis

**3.1.1 Particle size and zeta potential.** The particle size and PDI of the nanosuspension were found to be $179.6 \pm 1.16$ nm and $0.163 \pm 0.01$, respectively. The zeta potential of the nanosuspension was $-14.2 \pm 0.55$ mV. The polydispersity index (PDI) at $0.163 \pm 0.01$ (<0.2) showed that there is uniform size distribution of the nanoparticles. Small particles of uniform size are required to form microneedles with satisfactory strength and uniform drug content. The measured zeta potential value predicts the stability of the nanosuspension.

**3.1.2 Saturated solubility.** The saturated solubility values of pure carvedilol and carvedilol nanosuspension were found to be $6 \pm 0.04$ μg mL$^{-1}$ and $55.3 \pm 0.39$ μg mL$^{-1}$, respectively. There was a 9.21-fold increase in the saturation solubility of carvedilol in the nanosuspension form. An increase in solubility ultimately leads to higher absorption in the systemic circulation with subsequent enhanced bioavailability. The increase in solubility was attributed to the enormous increase in the surface area due to a reduction in particle size.

**3.1.3 TEM analysis.** The results of the TEM analysis of the carvedilol nanosuspension are shown in Fig. 1. The particle

size was found to be 181 nm, which correlates with the particle size analysis results.

**3.1.4 X-Ray diffraction (XRD).** The XRD results for pure carvedilol and carvedilol nanosuspension are shown in Fig. 2 and 3, respectively. It was observed that specific peaks of carvedilol at a specific $2\theta$ value were not present in the nanosuspension. The XRD indicates the alteration in the crystalline state of the drug after processing.

**3.1.5 Element analysis (EDS).** The EDS report on the optimized nanosuspension is shown in Fig. 4, which shows that zirconium is absent in the formulation. Thus, it can be said that there was no leaching of zirconium from the zirconium oxide beads. This eliminates the risk of toxicity due to zirconium.

## 3.2 Results and discussion of nanosuspension loaded microneedles

**3.2.1 Microscopy.** Optical microscopy images at 4× and 10× are shown in Fig. 4A and B, respectively. SEM images of microneedles are shown in Fig. 4C and D. The figures show well-formed microneedles with smooth surfaces. The tips are sharp, and this is required to adequately pierce the skin. Microneedle dimensions as per SEM are given in Table 1.
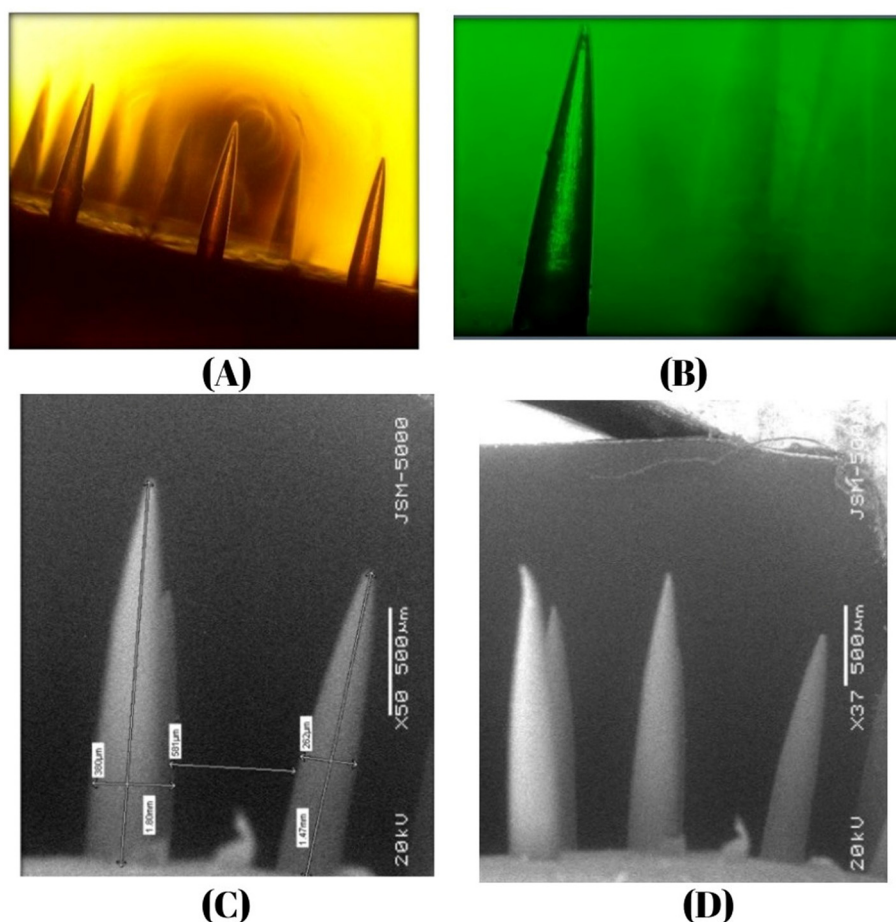


**Fig. 4** (A) SEM image of microneedles. Optical microscopy images at (B) 4× and (C) 10×. (D) SEM image of microneedles.

**RSC Pharmaceutics**

**3.2.2 Axial fracture force.** Fig. 5 shows the graph of load in grams *vs.* time in seconds. The first sharp peak was observed at a load of 547 g, which was the axial needle fracture force in grams. This value was converted into Newtons and gave the force exerted for needle failure. The AFF value obtained was 5.36 N. Successful piercing of the skin will occur if the AFF value is greater than 0.5.

**3.2.3 *In vitro* dissolution study.** Microscopic images of microneedles at different time points are shown in Fig. 6. They indicate that the dissolution of MN increased with time.

**3.2.4 Drug content.** The total drug content in the microneedle patch was found to be 98.78 ± 0.12%. The amount of drug per microneedle patch was found to be 3 mg.

**3.2.5 *In vitro* drug release study.** After 24 h, 93 ± 1.52% of the drug was released from the microneedle patch, which is given in Fig. 7. The *in vitro* drug release from the microneedle patch was analyzed using different pharmacokinetic models, and the correlation coefficient ($R^2$) values of the optimized batch for different kinetic models are given in Table 2. The highest $R^2$ value was found in the zero-order model, which shows that drug release was constant, irrespective of drug concentration. Zero-order release kinetics refers to the process of constant drug release from a formulation. There was a constant drug release over 24 hours, which signifies the possibility of a once-a-day microneedle application.

**3.2.6 Drug permeation and deposition study.** Transdermal patches containing microneedles and without microneedles were evaluated for drug permeation and drug deposition. After 24 hours, the % CDR from the simple patch was found to be 47.12 ± 0.11%, while from microneedles patch, it was 69.34 ± 0.24%. Fig. 8 shows the comparison of *ex vivo* drug release from the simple patch and microneedle patch. Both of their slopes represent steady-state flux across the skin. The steady-state flux for the plain patch was found to be 1.91 ± 1.55 µg cm$^{-2}$ h$^{-1}$, while for the microneedles patch, it was found to be 2.78 ± 0.62 µg cm$^{-2}$ h$^{-1}$.

$$\text{Penetration enhancement ratio : (PER)}$$
$$= \frac{J_{ss}(\text{microneedle})}{J_{ss}(\text{patch})} = 1.45$$

Thus, permeation was found to be increased by 1.45-fold by the microneedles patch. Image 11 shows a comparison of the drug deposition across the skin by the simple transdermal patch as well as the microneedles patch. The MN patch delivered 95.6 ± 0.77%, and in transdermal patches without MNs, it was found to be 66.29 ± 0.39% drug deposition across and within the skin. This indicates that greater drug permeation occurred from the MN patch due to the formation of micro-
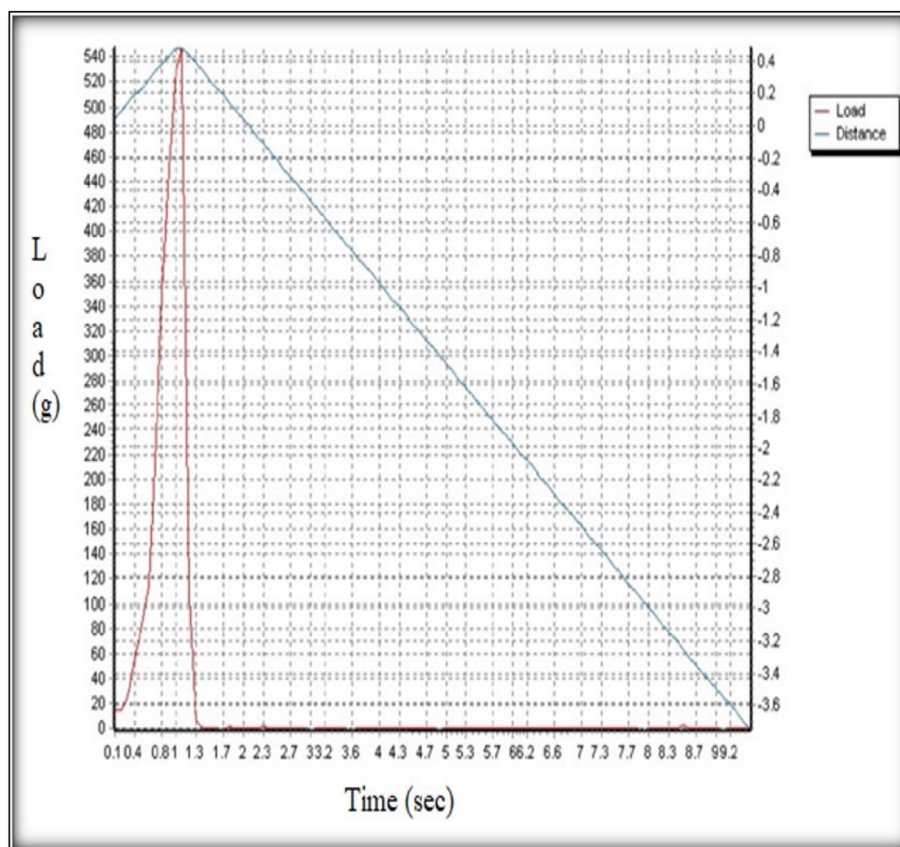


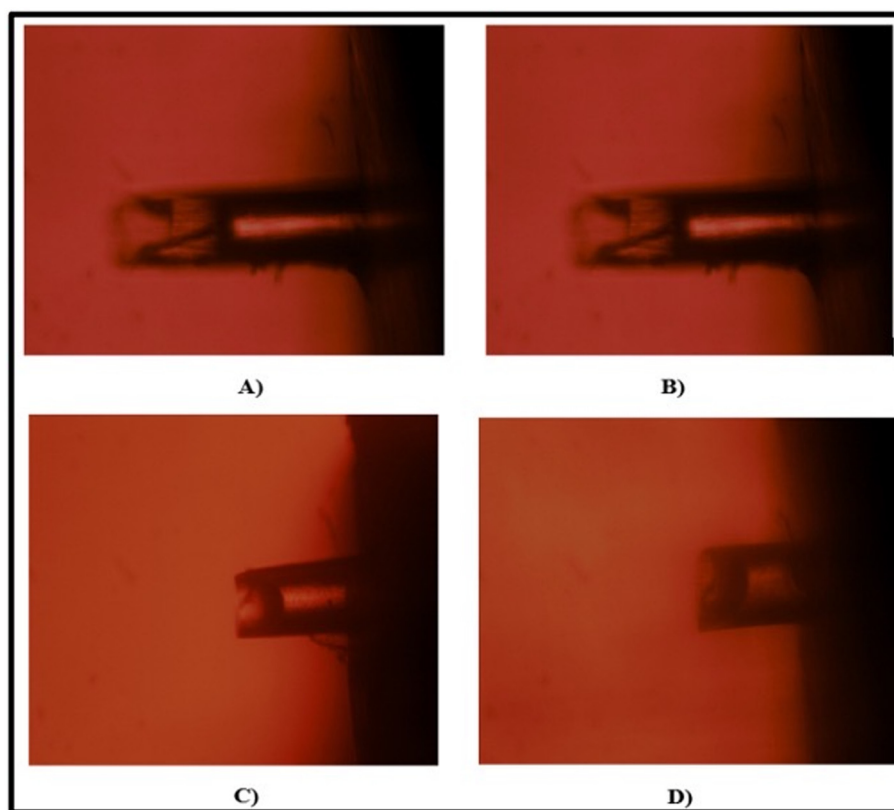**Fig. 5** Graph of grams *vs.* time for the measurement of the axial fracture force.

**Fig. 6** Microscopic images of microneedles at different time points. At (A) 5 minutes, (B) 10 minutes, (C) 15 minutes, and (D) 20 minutes.
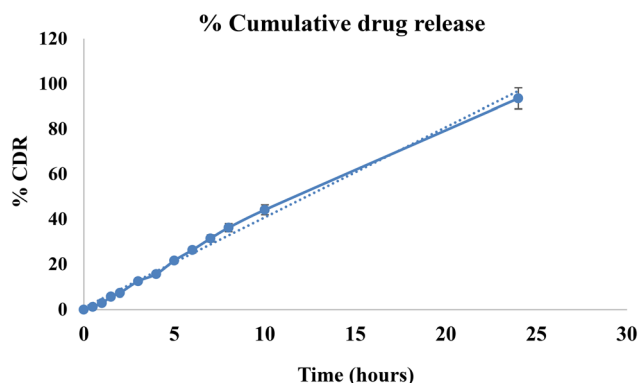


**Fig. 7** Cumulative drug release from microneedles.



**Fig. 8** Comparison of % CDR of a simple patch and a microneedle patch.

channels in the skin. The amount of drug retained on the surface of the skin was significantly lower in the case of a microneedle patch, which indicates the ability of microneedles to increase the penetration of drug across the skin.

**3.2.7 Histopathology study.** Image 9 shows a transverse section of skin treated with IPA, PBS (pH 7.4), drug suspension, or MN patch. IPA-treated skin was used as a positive control, and damage to the skin cells occurred. PBS (pH 7.4)-treated skin was used as a negative control, and healthy skin cells were observed. The haematoxylin and eosin-stained sections of rat abdominal skin treated with the developed micro-
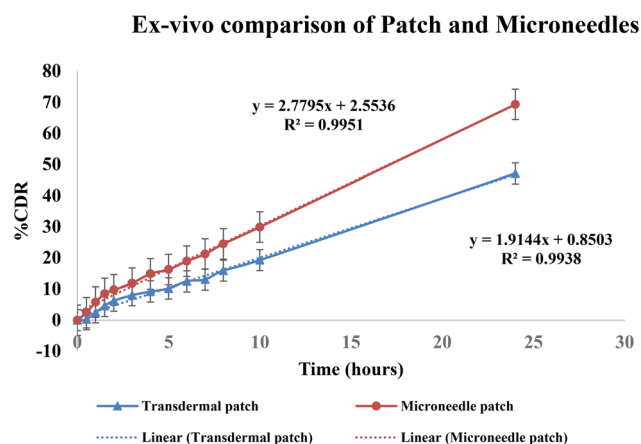
needle patch were examined under a microscope for any pathological changes and compared with the negative (PBS pH 7.4) and positive (IPA) controls to study the safety aspects of using a microneedle patch. The microneedle-treated skin, as well as the drug suspension-treated skin, showed the proper skin integrity when compared to the negative and positive control. Microneedle-treated skin showed cell integrity similar to that of the negative control. The microchannels are visible in the
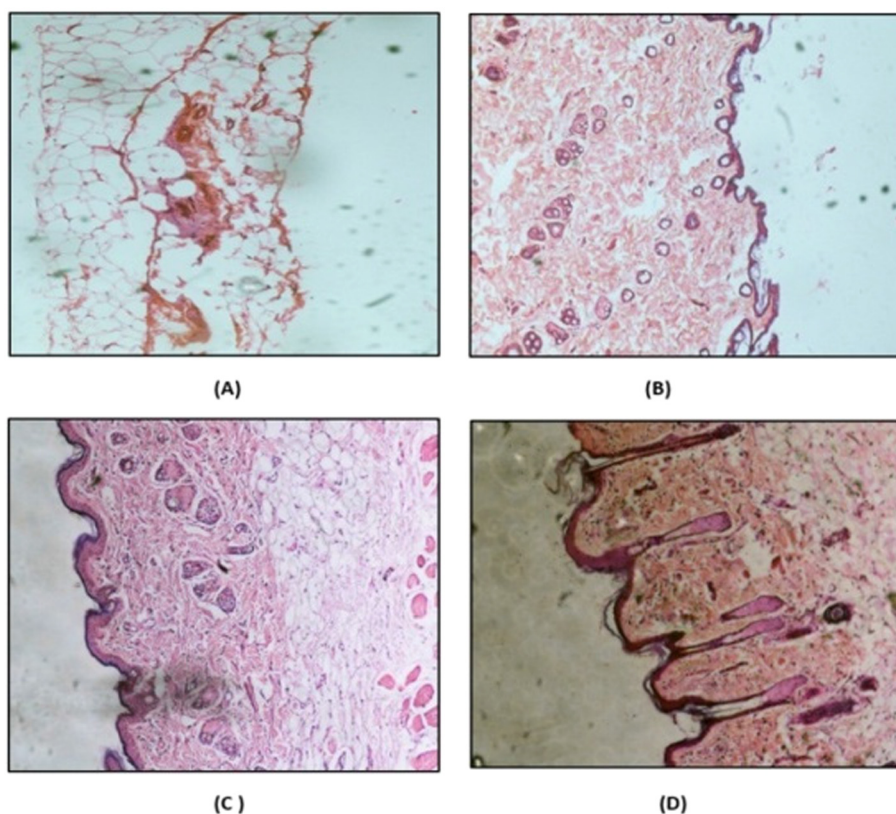
**Fig. 9** Histopathology images of (A) IPA (positive control), (B) PBS pH 7.4 (negative control), (C) drug suspension, and (D) microneedle patch.

case of microporated skin. Fig. 9D indicates the creation of microchannels in the skin due to the application of microneedles.

**3.2.8 *In vivo* pharmacokinetic studies.** Fig. 10 shows a comparison of the *in vivo* pharmacokinetic studies of marketed oral tablets, simple patches, and microneedle patches. It can

be concluded that the microneedle patch provided sustained release as compared to the marketed oral tablet. The parameters investigated for the pharmacokinetic studies are listed in Table 3, which shows that the $C_{max}$ obtained after transdermal application of the patch was significantly higher than that of oral administration. The absorption for carvedilol is lower after oral administration due to its low solubility and high first-pass metabolism. First-pass metabolism does not occur when a transdermal route of delivery is used, and hence, a higher $C_{max}$ was obtained. The $C_{max}$ obtained for microneedle patch was significantly higher than that of the simple patch, which indicated higher penetration through the skin. The relative bioavailability of the simple patch and microneedle patch was 1.32-and 2.82-fold higher compared to the marketed oral formulation, respectively. The enhanced bioavailability was attributed to the elimination of first-pass metabolism. This leads to the possibility of a reduction in the dose, and consequently, a reduction in drug side effects. The MRT for microneedle patch was also significantly higher compared to the simple patch and oral formulation because of the sustained release of the drug from the microneedles. Upon calculating the relative bioavailability, it was found that the bioavailability of the microneedle patch was enhanced by 2.82-fold as compared to the oral marketed tablet. Additionally, the relative bioavailability of the microneedle patch was 2 times greater than that of the simple transdermal patch (Fig. 11).
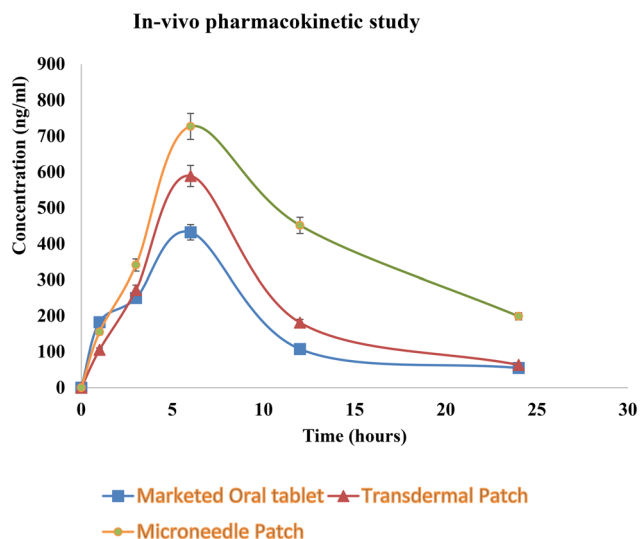


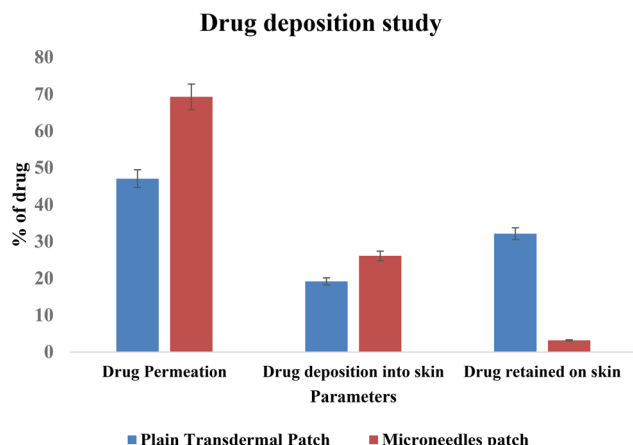**Fig. 10** *In vivo* pharmacokinetic study.

**Fig. 11** Skin permeation and deposition study.

**3.2.9 Stability studies.** The effect of various storage conditions such as temperature and humidity on carvedilol microneedles is shown in Table 4. The insignificant change in drug content under both storage conditions indicates the stability of the drug in the prepared microneedle formulation. The reduction in axial fracture force value indicates moisture uptake by the microneedles. There was a slight decrease in the drug release from the microneedle patch, but it was able to deliver more than 85% of the drug in 24 hours.

# 4. Conclusion

A microneedle patch containing a carvedilol nanosuspension was developed and optimized using $3^2$ full factorial designs. Carvedilol nanosuspension and carvedilol MN patches possess desirable characteristics that were confirmed by different evaluation tests. The microneedle patch led to significant enhancement of carvedilol bioavailability through the transdermal route. The drug release from the microneedles followed zero order kinetics, which is desirable in the case of transdermal delivery. The sustained release of the drug coupled with higher bioavailability leads to the possibility of reduction in dose and dosing frequency. Thus, the developed transdermal microneedle patch to administer carvedilol nanosuspension seems to be the promising and more patient-compliant approach for the management of hypertension.

# Author contributions

Anushri Deshpande: literature review for project selection conception, performing the laboratory experiments, and analyzing the results. Vidhi Mer: preparation of the draft manuscript. Darshana Patel: checking and revising the draft manuscript. Hetal Thakkar: providing overall guidance for project selection, manuscript preparation, final approval of the manuscript for communication, and final approval of the version to be communicated.

# Conflicts of interest

There are no conflicts to declare.

# Acknowledgements

# References

1 R. R. Arun and J. Harindran, Enhancement of bioavailability of carvedilol using solvent deposition techniques, *Int. J. Pharm. Sci. Res.*, 2017, **8**(8), 3391–3401.

2 P. C. Stafylas and P. A. Sarafidis, Carvedilol in hypertension treatment, *Vasc. Health Risk Manage.*, 2008, **4**(1), 23.

3 B. N. Nalluri, *et al.*, Controlled release tablet formulations of carvedilol, *J. Chem. Pharm. Res.*, 2012, **4**, 4266–4274.

4 A. M. Gupta and U. Shivhare, FORMULATION, AND Characterisation of Sustained Release Carvedilol Tablet from Reservoir Pellets, *Int. J. Pharm. Sci. Res.*, 2016, 7(2), 626.

5 V. K. Venishetty, *et al.*, Design and evaluation of polymer coated carvedilol loaded solid lipid nanoparticles to improve the oral bioavailability: a novel strategy to avoid intraduodenal administration, *Colloids Surf., B*, 2012, **95**, 1–9.

6 G. Arzani, *et al.*, Niosomal carriers enhance oral bioavailability of carvedilol: effects of bile salt-enriched vesicles and carrier surface charge, *Int. J. Nanomed.*, 2015, **10**, 4797.

7 B. Singh, *et al.*, Optimized nanoemulsifying systems with enhanced bioavailability of carvedilol, *Colloids Surf., B*, 2013, **101**, 465–474.

8 D. Liu, *et al.*, Controlled delivery of carvedilol nanosuspension from osmotic pump capsule: in vitro and in vivo evaluation, *Int. J. Pharm.*, 2014, **475**(1–2), 496–503.

9 K. Yuvaraja and J. Khanam, Enhancement of carvedilol solubility by solid dispersion technique using cyclodextrins, water-soluble polymers, and hydroxyl acid, *J. Pharm. Biomed. Anal.*, 2014, **96**, 10–20.

10 H. P. Thakkar, B. V. Patel and S. P. Thakkar, Development and characterization of nanosuspensions of olmesartan medoxomil for bioavailability enhancement, *J. Pharm. BioAllied Sci.*, 2011, **3**(3), 426.

11 V. Patravale, A. A. Date and R. Kulkarni, Nanosuspensions: a promising drug delivery strategy, *J. Pharm. Pharmacol.*, 2004, **56**(7), 827–840.

12 M. G. Nava-Arzaluz, *et al.*, Microneedles as transdermal delivery systems: combination with other enhancing strategies, *Curr. Drug Delivery*, 2012, **9**(1), 57–73.

13 P. R. Nivrutti, P. A. Nath and J. H. Anantrao, Drug penetration enhancement techniques in transdermal drug delivery system: A review, *J. Pharm. Res. Int.*, 2021, **33**(19B), 46–61.

14 Y. Wang, *et al.*, Influencing factors and drug application of iontophoresis in transdermal drug delivery: an overview of recent progress, *Drug Delivery Transl. Res.*, 2022, **12**(1), 15–26.

15 B. C.-Q. Seah and B. M. Teo, Recent advances in ultrasound-based transdermal drug delivery, *Int. J. Nanomed.*, 2018, **13**, 7749.

16 N. Khare and P. Shende, Microneedle system: A modulated approach for penetration enhancement, *Drug Dev. Ind. Pharm.*, 2021, **47**(8), 1183–1192.

17 T. Haque and M. M. U. Talukder, Chemical enhancer: a simplistic way to modulate barrier function of the stratum corneum, *Adv. Pharm. Bull.*, 2018, **8**(2), 169.

18 M. M. D. C. Lobita, *Development of dissolving microneedles for delivery of cancer cells membrane antigens*, 2021.

19 V. Alimardani, *et al.*, Recent advances on microneedle arrays-mediated technology in cancer diagnosis and therapy, *Drug Delivery Transl. Res.*, 2021, **11**(3), 788–816.

20 H. Wei, *et al.*, Hydrogel-based microneedles of chitosan derivatives for drug delivery, *React. Funct. Polym.*, 2022, **172**, 105200.

21 H. X. Nguyen, *et al.*, Poly (vinyl alcohol) microneedles: Fabrication, characterization, and application for transdermal drug delivery of doxorubicin, *Eur. J. Pharm. Biopharm.*, 2018, **129**, 88–103.

22 K. D. Koradia, *et al.*, Ziprasidone nanocrystals by wet media milling followed by spray drying and lyophilization: Formulation and process parameter optimization, *J. Drug Delivery Sci. Technol.*, 2018, **43**, 73–84.

23 Q. L. Wang, *et al.*, A fabrication method of microneedle molds with controlled microstructures, *Mater. Sci. Eng., C*, 2016, **65**, 135–142.

24 H. Thakkar, K. Pandya and B. Patel, Microneedle-mediated transdermal delivery of tizanidine hydrochloride, in *Drug Delivery Systems*, Springer, 2020, pp. 239–258.

25 S. K. Sukumaran and C. Venkatasubramaniyan, Design and Development of Chitosan Based Etravirine Nanosuspension, *Nanomed. Res. J.*, 2022, **7**(3), 270–287.

26 Q. Liu, *et al.*, A wet-milling method for the preparation of cilnidipine nanosuspension with enhanced dissolution and oral bioavailability, *J. Drug Delivery Sci. Technol.*, 2020, **55**, 101371.

27 L. K. Vora, *et al.*, Novel nanosuspension–based dissolving microneedle arrays for transdermal delivery of a hydrophobic drug, *J. Interdiscip. Nanomed.*, 2018, **3**(2), 89–101.

28 H. Kathuria, *et al.*, Large size microneedle patch to deliver lidocaine through the skin, *Pharm. Res.*, 2016, **33**(11), 2653–2667.

29 A. Dąbrowska, *et al.*, A water-responsive, gelatine-based human skin model, *Tribol. Int.*, 2017, **113**, 316–322.

30 H. P. Thakkar, H. Savsani and P. Kumar, Ethosomal hydrogel of raloxifene HCl: statistical optimization & ex vivo permeability evaluation across microporated Pig ear skin, *Curr. Drug Delivery*, 2016, **13**(7), 1111–1122.

31 S. Amodwala, P. Kumar and H. P. Thakkar, Statistically optimized fast dissolving microneedle transdermal patch of meloxicam: A patient-friendly approach to manage arthritis, *Eur. J. Pharm. Sci.*, 2017, **104**, 114–123.